Monthly Notices of the ROYAL ASTRONOMICAL SOCIETY

MNRAS **535,** 2482–2493 (2024) https://doi.org/10.1093/mnras/stae2496
Advance Access publication 2024 November 6

The X-ray re-brightening of GRB afterglow revisited: a possible signature from activity of the central engine

Zhe Yang,[1] Hou-Jun Lü [1]★ Xing Yang,[1] Jun Shen[2] and Shuang-Xi Yi [3]

[1]*Guangxi Key Laboratory for Relativistic Astrophysics, School of Physical Science and Technology, Guangxi University, Nanning 530004, China*
[2]*Institute of Astrophysics, Central China Normal University, Wuhan 430079, China*
[3]*School of Physics and Physical Engineering, Qufu Normal University, Qufu 273165, China*

Accepted 2024 October 31. Received 2024 October 31; in original form 2023 September 12

ABSTRACT

Long-duration gamma-ray bursts (GRBs) are thought to be from core collapse of massive stars, and a rapidly spinning magnetar or black hole may be formed as the central engine. The extended emission in the prompt emission, flares, and plateaus in X-ray afterglow, are proposed to be as the signature of central engine re-activity. However, the direct evidence from observations of identifying the central engines remains an open question. In this paper, we systemically search for long-duration GRBs that consist of bumps in X-ray afterglow detected by *Swift*/XRT and find that the peak time of the X-ray bumps exhibit bimodal distribution (defined as 'early' and 'late' bumps) with division line at $t = 7190$ s. Although we cannot rule out that such a bimodality arises from selection effects. We proposed that the long-duration GRBs with an early (or late) bumps may be originated from the fall-back accretion onto a new-born magnetar (or black hole). By adopting Monte Carlo Markov Chain (MCMC) method to fit the early (or late) bumps of X-ray afterglow with the fall-back accretion of magnetar (or black hole), it is found that the initial surface magnetic field and period of magnetars for most early bumps are clustered around 5.88×10^{13} G and 1.04 ms, respectively. Meanwhile, the derived accretion mass of black hole for late bumps is in the range of $[4 \times 10^{-4}, 1.8 \times 10^{-2}]\,M_{\odot}$, and the typical fall-back radius is distributed range of $[1.04, 4.23] \times 10^{11}$ cm, which is consistent with the typical radius of a Wolf–Rayet star. However, we also find that the fall-back accretion magnetar model is disfavoured by the late bumps, but the fall-back accretion of black hole model cannot be ruled out to interpret the early bumps of X-ray afterglow.

Key words: (transients:) gamma-ray bursts.

1 INTRODUCTION

In general, it is believed that gamma-ray bursts (GRBs) originated from the collapsar of massive stars or the merger of double compact stars (Eichler et al. 1989; Woosley 1993; MacFadyen & Woosley 1999; Zhang 2018). Within both the collapsar and compact-star merger models, a hyperaccretion black hole or a rapidly spinning, strongly magnetized neutron star (millisecond magnetar) as the central engine may be formed, and it launches a relativistic outflow (Usov 1992; Dai & Lu 1998a,b; Popham, Woosley & Fryer 1999; Narayan, Piran & Kumar 2001; Zhang & Mészáros 2001; Fan & Xu 2006; Chen & Beloborodov 2007; Metzger et al. 2010; Lei, Zhang & Liang 2013; Lü & Zhang 2014; Lü et al. 2015). The observed prompt gamma-ray emission is explained by the fireball internal shocks (Rees & Meszaros 1994), dissipated photosphere models (Thompson 1994; Rees & Mészáros 2005; Pe'er, Mészáros & Rees 2006), and the internal-collision-induced magnetic re-connection and turbulence (ICMART) model (Zhang & Yan 2011). The broad-band afterglow emission is produced from forward and reverse external shocks when the fireball is decelerated by a circumburst medium (Mészáros & Rees 1997; Sari, Piran & Narayan 1998; Kobayashi 2000; Mészáros 2002; Zhang & Mészáros 2004; Zhang, Lü & Liang 2016).

However, how to identify the central engine (black hole or magnetar) of GRBs remain an open question (Zhang 2011). From the observational point of view, some GRBs have been discovered to exhibit a plateau emission component or an extremely steep drop following the plateau (known as internal plateaus) in their X-ray afterglows (O'Brien et al. 2006; Zhang et al. 2006; Liang, Zhang & Zhang 2007; Troja et al. 2007; Lyons et al. 2010; Rowlinson et al. 2010, 2013; Lü & Zhang 2014; Lü et al. 2015), which is consistent with millisecond magnetar central engine (Usov 1992; Dai & Lu 1998a,b; Zhang & Mészáros 2001). On the other hand, non-plateau emission in the afterglows, the released energy of GRB exceeded the energy budget of magnetar, or the later giant bump in the afterglows, are inconsistent with the magnetar central, but can be interpreted by black hole central engine, such as GRBs 121027A and 111209A (Kumar, Narayan & Johnson 2008; Wu, Hou & Lei 2013; Yu et al. 2015; Lü et al. 2018; Zhao et al. 2021).

From the theoretical point of view, Zhang & Dai (2008, 2009) invoked a new-born neutron star surrounded by hyperaccretion and neutrino cooling disc to produce both GRB jet and observed plateau emission. Within this scenario, Dai & Liu (2012) proposed a hyperaccretion fall-back disc around a newborn millisecond magnetar model to produce a significant brightening of an early afterglow (early X-ray bump) when magnetar is spin-up due to a sufficient angular momentum of the accreted matter transferred to the magnetar. If

★ E-mail: lhj@gxu.edu.cn

the central engine is a black hole, a giant X-ray or optical bump can be produced via the fall-back of black hole when the duration and accretion rate of black hole fallback are long and large enough, respectively (Wu et al. 2013; Yu et al. 2015; Lü et al. 2018; Zhao et al. 2021). If this is the case, different types of central engine of GRBs may produce different characteristics of X-ray or optical afterglows.

In this paper, we systematically search for long-duration GRBs with an early and later X-ray bumps emission from the *Swift*-X-Ray Telescope (XRT) GRB sample, and try to interpret both early and later X-ray bumps by invoking fall-back accretion of magnetar and black hole, respectively. The criteria of sample selection and the data reduction are presented in Section 2. In Section 3, we described the basic models of both spin-up of magnetar fall-back and the black hole fall-back accretion. We apply the two models to fit the early and later X-ray afterglow of GRBs, respectively, in Section 4. Our conclusions and discussion are given in Section 5. Throughout the paper, a concordance cosmology with parameters $H_0 = 71\,\mathrm{km\,s^{-1}\,Mpc^{-1}}$, $\Omega_\mathrm{M} = 0.30$, and $\Omega_\Lambda = 0.70$ is adopted.

2 DATA REDUCTION AND SAMPLE SELECTION CRITERIA

The XRT data are downloaded from the Swift data archive (Evans et al. 2007).[1] Our entire sample includes more than 1718 GRBs observed by *Swift*/XRT between 2005 January and 2023 July. We only focus on the long-duration GRBs with the bump emission in X-ray afterglow and analyse 1043 long-duration GRBs. Among these, 154 GRBs are too faint to be detected in the X-ray band, or do not have enough photons to extract a reasonable X-ray light curve. Then, we select the GRBs that X-ray emission exhibit the feature of rise and fall and adopt a smooth broken power-law function to fit (Liang et al. 2007; Lü et al. 2022),

$$F_1(t) = F_{01}\left[\left(\frac{t}{t_\mathrm{p}}\right)^{\omega\alpha_1} + \left(\frac{t}{t_\mathrm{p}}\right)^{\omega\alpha_2}\right]^{-1/\omega}, \quad (1)$$

$$F_2(t) = \left(F_1^{-\omega_1} + F_3^{-\omega_1}\right)^{-1/\omega_1}, \quad (2)$$

$$F_3(t) = F_2(t_{\mathrm{b},2})\left(\frac{t}{t_{\mathrm{b},2}}\right)^{-\alpha_3}, \quad (3)$$

where fixed $\omega = \omega_1 = 3$ represents the sharpness of the peak and t_p, α_1, and α_2 are the peak time, and the rising and decay slopes of X-ray variability, respectively.

Since the X-ray flares have been discovered in a good fraction of *Swift* GRBs (Burrows et al. 2005; Chincarini et al. 2007; Margutti et al. 2010). Their light curves are typically narrow and show rapid rise and fall with steep rising and decaying indices. This feature of X-ray flares is similar to that of prompt emission and suggests that the X-ray flares are likely to share a similar mechanism with the prompt emission, such as internal dissipation of long-lasting central engine activity (Burrows et al. 2005; Liang et al. 2006; Nousek et al. 2006; Zhang et al. 2006; Troja et al. 2015; Yi et al. 2016). Yi et al. (2016) performed a systematic study of X-ray flares observed by *Swift* to obtain the rising and decaying indices and found that the rising and decaying indices of those flares are larger or much larger than 3. While we find that a small fraction of GRBs x-ray afterglow whose rising and decaying indices are less than 3 (called X-ray bump). It means that the physical origin of those X-ray bumps may be different from that of X-ray flares, and it is possible related to the central central engine, e.g. spin-up of magnetar or fall-back of black hole.

In general, the X-ray emission of GRBs is very complicated Zhang et al. (2006). Since the steep decay segment with a power-law decay is from the curvature effect as the prompt emission tail. The light curves of X-rays are considered to fit by the initial steep decay component, afterglow component (e.g. from external shock) with power-law decay, smooth broken power-law segment (bumps), as well as the post-jet segment if it needs possible. Our sample does not include the cases in Yi et al. (2016), who performed a systematic study and defined the X-ray flares. So that, excepting the GRBs that are in Yi et al. 2016, three criteria are adopted for our sample selection. (i) the rising and decay slopes of X-ray bumps are required to be less than that of X-ray flares defined in Yi et al. (2016). (ii) the duration of X-ray bumps should be longer and wider than that of X-ray flares in Yi et al. (2016). (iii) in order to extract the X-ray light curve, the observed X-ray light curve should be at least more than 5 data points. By accepting the above criteria, our sample therefore only comprises 28 long-duration GRBs, including 17 GRB with redshift measured. Fig. 1 shows two examples of the fitting results with smooth broken power-law function and other components.[2] The fitting results are presented in Table 1, it includes the rising and decay slopes of bumps, peak times, and the start and end times of bumps.

Fitting the X-ray light curve with a broken power-law model, one finds that peak time of X-ray bumps exhibits bimodal distribution with peak times as $t_{\mathrm{p},1} = 1273 \pm 686\,\mathrm{s}$ and $t_{\mathrm{p},2} = 21752 \pm 8566\,\mathrm{s}$, respectively. The division line is at $t = 7190\,\mathrm{s}$ (see Fig. 1). So that, we classify the X-ray bumps as two categories, e.g. 'early' bumps with $t_\mathrm{p} < 7190\,\mathrm{s}$, and 'late' bumps with $t_\mathrm{p} > 7190\,\mathrm{s}$, respectively. Moreover, one needs to clarify that the bimodal distribution of peak times can be affected by the selection effect, namely, the number of what we selected sample may be a sun-class of total GRBs observed by *Swift*/XRT. On the other hand, it is also possible affected by the sheltering from Earth, namely, the dip of bimodal distribution of apparent peak times is possible caused by the selection effect due to sheltered time from Earth.

3 MODELS DESCRIPTION OF MAGNETAR AND BLACK HOLE FALL-BACK ACCRETION

In this section, we will present more details in theory for fall-back accretion onto a new-born magnetar and black hole, respectively.

3.1 Hyperaccretion fall-back disc around a newborn millisecond magnetar model

A millisecond magnetar may survive as the central engine of long-duration GRBs after the massive star collapse. A small fraction of ejecta cannot escape from the system due to the gravity of central magnetar, and it will fall back to the surface of magnetar. If this is the case, the central magnetar will spin up again when the accumulated materials on the surface of magnetar is large enough. The fall-back accretion onto a new-born magnetar is also used to interpret the early X-ray and optical bumps in the GRB afterglow (Dai & Lu 1998a,b; Dai & Liu 2012; Yu et al. 2015; Zhong et al. 2016). Roughly estimated, the minimum time-scale of fall-back is equal to free-fall time-scale. In fact, the time-scale of fall-back is affected by many factors (MacFadyen, Woosley & Heger 2001; Dai & Liu 2012). In our

[1] http://www.swift.ac.uk/archive/obs.php?burst = 1.

[2] https://astro.gxu.edu.cn/info/1062/2243.htm

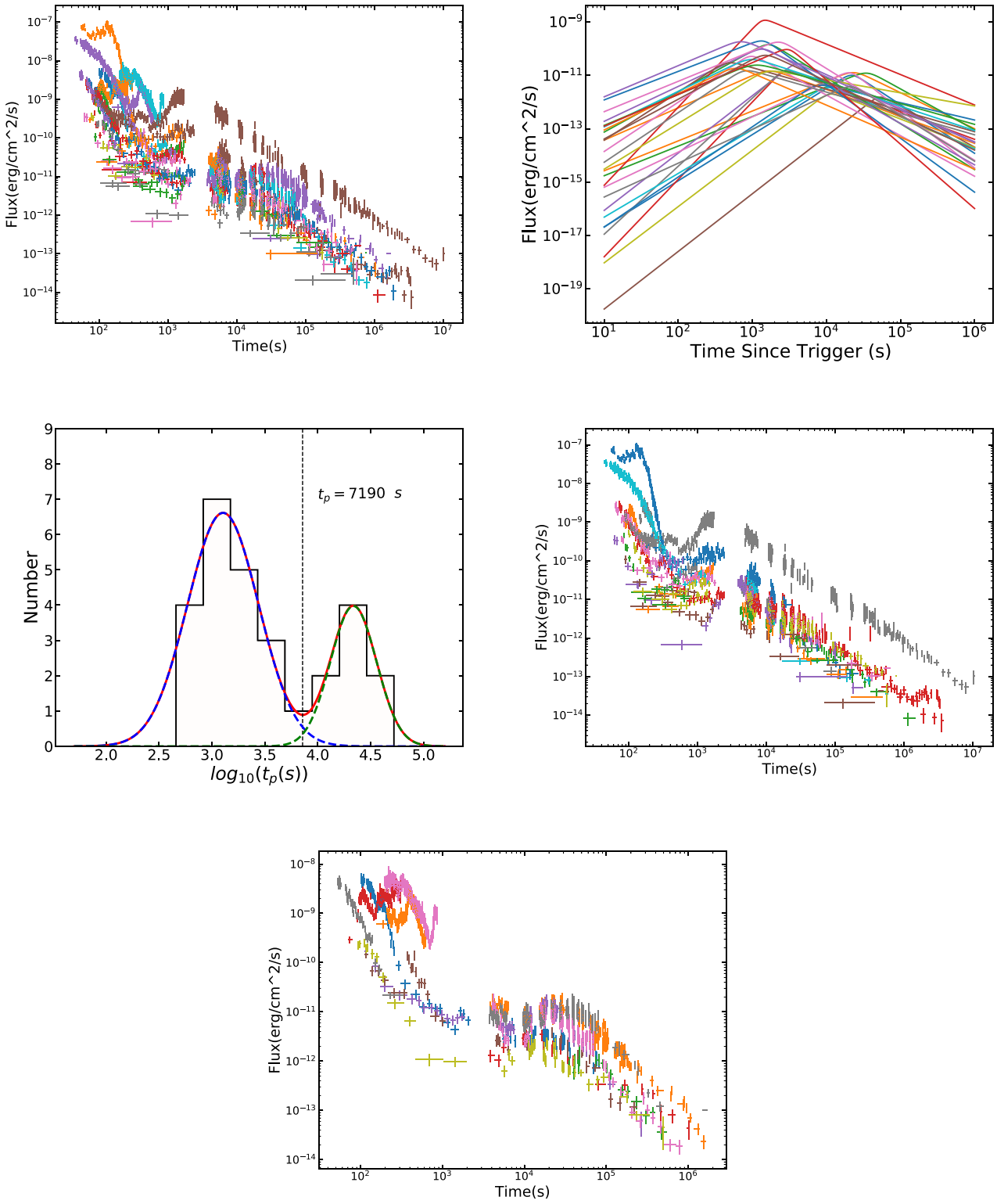

Figure 1. (a) X-ray light curves of our total sample. (b) Fits of our sample with the broken power-law model. (c) Histogram of the peak time distribution for our sample. The dashed lines are the Gaussian fits. (d) X-ray light curves of early bumps. (e) X-ray light curves of late bumps.

calculations, we adopt $t_0 \sim 10^2$ s, which is derived from numerical simulations as the starting time of materials fall-back (MacFadyen et al. 2001).

Following the method in MacFadyen et al. (2001) and Zhang & Dai (2008), the acceleration rate of fall-back can be expressed as

$$\dot{M} = \left(\dot{M}_{\rm early}^{-1} + \dot{M}_{\rm late}^{-1}\right)^{-1}, \quad (4)$$

Table 1. The fitting results of our sample with smooth broken power-law model.

GRB Name	T_{90} (s)	$T_{\rm start}$ (s)	$T_{\rm end}$ (s)	$t_{\rm p}$ (s)	α_1	α_2	z	References[a]
Early bump								
051016B	4.0	320	13 500	776^{+703}_{-263}	$0.80^{+0.07}_{-0.05}$	$-1.86^{+0.25}_{-0.31}$	0.9364	(1)
060206	7.0	1200	12 900	3981^{+1030}_{-818}	$1.26^{+0.04}_{-0.04}$	$-2.15^{-1.15}_{0.82}$	4.048	(2)
070208	48.0	180	14 000	954^{+45}_{-63}	$1.52^{+0.21}_{-0.30}$	$-1.85^{+0.01}_{-0.05}$	1.165	(3)
090429B	5.5	120	16 800	588^{+262}_{-121}	$1.20^{+0.15}_{-0.12}$	$-1.36^{+0.28}_{-1.21}$	9.4	(4)
091029	39.2	525	18 900	1548^{+2524}_{-1202}	$0.49^{+0.09}_{-0.06}$	$-1.71^{+0.20}_{-0.15}$	2.752	(5)
120118B	23.3	320	11 000	1659^{+290}_{-247}	$1.01^{0.12}_{0.10}$	$-1.21^{+0.16}_{-0.39}$	2.943	(6)
120213A	48.9	620	12 000	3096^{+298}_{-336}	$2.41^{+0.36}_{-0.32}$	$-1.19^{+0.14}_{-0.34}$	–	–
120224A	8.1	220	19 000	1071^{+227}_{-220}	$0.78^{+0.08}_{-0.06}$	$-1.16^{+0.12}_{-0.34}$	–	–
121209A	42.7	100	7000	707^{+104}_{-76}	$1.23^{+0.06}_{-0.06}$	$-1.17^{+0.13}_{-0.33}$	–	–
140515A	23.4	580	14 800	2691^{+470}_{-179}	$1.03^{+0.08}_{-0.06}$	$-2.90^{+0.79}_{-0.61}$	6.32	(7)
150911A	7.2	280	24 800	1479^{+811}_{-330}	$1.29^{+0.64}_{-0.27}$	$-1.49^{+1.38}_{-1.05}$	–	–
161129A	35.53	100	25 000	1412^{+172}_{-153}	$2.02^{+0.22}_{-0.22}$	$-1.07^{+0.05}_{-0.18}$	0.645	(8)
170202A	46.2	300	59 300	933^{+163}_{-138}	$0.91^{+0.03}_{-0.04}$	$-1.31^{+0.21}_{-0.35}$	3.645	(9)
170822A	64.0	500	19 300	2344^{+167}_{-156}	$1.72^{+0.10}_{-0.11}$	$-1.14^{+0.10}_{-0.28}$	–	–
181110A	138.4	400	36 300	1659^{+290}_{-247}	$1.72^{+0.13}_{-0.10}$	$-1.52^{+0.39}_{-0.89}$	1.505	(10)
190829A	58.2	500	56 300	1380^{+65}_{-31}	$1.14^{-0.02}_{+0.02}$	$-2.93^{+0.31}_{-0.32}$	0.078	(11)
200917A	19.4	1000	36 300	2754^{+793}_{-355}	$1.17^{+0.20}_{-0.17}$	$-2.55^{+1.07}_{-0.97}$	–	–
201128A	5.41	150	7300	457^{+58}_{-131}	$0.80^{+0.15}_{-0.07}$	$-1.80^{+1.02}_{-0.27}$	–	–
220117A	49.8	350	13 200	1380^{+133}_{-121}	$1.55^{+0.09}_{-0.08}$	$-1.31^{+0.21}_{-0.35}$	4.961	(12)
Late bump								
071010A	6.0	35 000	533 200	52480^{+7775}_{-51433}	$1.54^{+0.32}_{-0.41}$	$-2.16^{+2.16}_{-1.11}$	0.98	(13)
081028	260.0	9800	233 200	22387^{+1055}_{-1007}	$1.83^{+0.08}_{-0.08}$	$-1.73^{+0.25}_{-0.29}$	3.038	(14)
100901A	439.0	9680	33 320	23442^{+1104}_{-1564}	$1.35^{+0.05}_{-0.07}$	$-1.12^{+0.09}_{-0.23}$	1.408	(15)
120215A	26.5	5160	53 200	10964^{+2217}_{-1632}	$1.07^{+0.24}_{-0.17}$	$-2.11^{+0.71}_{-1.07}$	–	–
120326A	69.6	9560	330 200	35481^{+1672}_{-12039}	$1.53^{+0.11}_{-0.19}$	$-1.11^{+0.08}_{-1.00}$	1.798	(16)
130807A	37.7	3260	100 200	10471^{+2117}_{-2153}	$1.21^{+0.27}_{-0.22}$	$-1.64^{+0.44}_{-1.06}$	–	–
131018A	73.2	4350	100 000	7413^{+1707}_{-1387}	$0.65^{+0.12}_{-0.11}$	$-1.88^{+0.71}_{-1.43}$	–	–
150626B	48.0	5090	60 000	20892^{+1494}_{-1394}	$2.18^{+0.17}_{-0.17}$	$-1.32^{+0.22}_{-0.43}$	–	–
230414B	25.9	6490	69 500	21379^{+3167}_{-2758}	$1.73^{+0.15}_{-0.13}$	$-1.27^{+0.34}_{-0.03}$	3.568	(17)

Note.[a] The references of redshift for our sample. (1) Soderberg, Berger & Ofek (2005); (2) Fynbo et al. (2006); (3) Cucchiara et al. (2007); (4) Cucchiara et al. (2011); (5) Chornock, Perley & Cobb (2009); (6) Malesani et al. (2013); (7) Chornock, Fox & Berger (2014); (8) Cano et al. (2016); (9) Palmerio et al. (2017); (10) Perley et al. (2018); (11) Lipunov et al. (2019); (12) Palmerio et al. (2022); (13) Prochaska et al. (2007); (14) Berger et al. (2008); (15) Chornock et al. (2010); (16) Tello et al. (2012); (17) Agui Fernandez et al. (2023).

where

$$\dot{M}_{\rm early} = 10^{-3}\eta_{\rm mag}\, t^{1/2}\, {\rm M}_\odot\, {\rm s}^{-1} \tag{5}$$

and

$$\dot{M}_{\rm late} = 10^{-3}\eta_{\rm mag}\, t_1{}^{13/6}\, t^{-5/3}\, {\rm M}_\odot\, {\rm s}^{-1}. \tag{6}$$

Here, $\eta_{\rm mag} \sim 0.01$–10 is a factor that accounts for different explosion energies, and $t_1 \sim 200$–1000 s is similar to the time of peak flux of radiation generated by fall-back accretion (longer t_1 corresponding to smaller $\eta_{\rm mag}$). One roughly estimates $\dot{M} \propto t^{-5/3}$ if $t \gg t_1$ (Chevalier 1989). The gravitational mass (M) of the central magnetar can be obtained as Dai & Liu (2012),

$$M = M_{\rm b}(t)\left[1 + \frac{3}{5}\frac{GM_{\rm b}(t)}{R_{\rm s}c^2}\right], \tag{7}$$

and

$$M_{\rm b}(t) = M_0 + \int_0^t \dot{M}\, {\rm d}t, \tag{8}$$

Here, $R_{\rm s}$ and M_0 are the radius and the initial baryonic mass of the magnetar, respectively, $M_{\rm b}$ is the total baryonic mass of magnetar at time t.

Based on the results of Dai & Liu (2012), three radii are defined within the accretion disc, e.g. co-rotation radius ($r_{\rm c}$), magnetospheric radius ($r_{\rm m}$), and radius of light cylinder ($R_{\rm L}$). The r_c is defined as following when the rotating angular velocity ($\Omega_{\rm s}$) of the central engine is equal to Keplerian angular velocity ($\Omega_{\rm k}$),

$$r_{\rm c} = \left(\frac{GM}{\Omega_{\rm s}^2}\right)^{1/3}. \tag{9}$$

The magnetospheric radius $r_{\rm m}$ is

$$r_{\rm m} = \left(\frac{\mu^4}{GM\dot{M}^2}\right)^{1/7}, \tag{10}$$

where $\mu = B_0 R_{\rm s}^3$ is the magnetic dipole moment of the magnetar, and B_0 is the initial surface magnetic field of magnetar. The radius

Table 2. The MCMC fitting results of early bump subsample with fall-back accretion of magnetar.

GRB[a] Name	log t_l (s)	log η_{mag}	log (B_0) (G)	P_0 (ms)
051016B	$2.60^{+0.11}_{-0.11}$	$-2.06^{+0.18}_{-0.22}$	$13.69^{+0.04}_{-0.04}$	$1.11^{+0.13}_{-0.12}$
060206	$3.49^{+0.02}_{-0.02}$	$-1.88^{+0.02}_{-1.88}$	$13.72^{+0.03}_{-0.02}$	$1.48^{+0.34}_{-0.35}$
070208	$2.13^{+0.12}_{-0.09}$	$-1.12^{+0.16}_{-0.23}$	$13.74^{+0.02}_{-0.02}$	$1.34^{+0.30}_{-0.20}$
090429B	$2.67^{+0.08}_{-0.07}$	$-0.77^{+0.07}_{-0.07}$	$14.00^{+0.04}_{-0.05}$	$0.57^{+0.10}_{-0.05}$
091029	$3.26^{+0.06}_{-0.04}$	$-1.88^{+0.04}_{-0.05}$	$13.73^{+0.03}_{-0.03}$	$15.42^{+10.33}_{-6.71}$
120118B	$2.58^{+0.21}_{-0.13}$	$-1.83^{+0.24}_{-0.43}$	$13.60^{+0.03}_{-0.03}$	$1.19^{+0.25}_{-0.18}$
120213A*	$3.36^{+0.03}_{-0.03}$	$-2.16^{+0.04}_{-0.04}$	$13.96^{+0.03}_{-0.06}$	$1.33^{+0.45}_{-0.32}$
120224A*	$2.76^{+0.24}_{-0.20}$	$-2.03^{+0.31}_{-0.31}$	$13.58^{+0.03}_{-0.03}$	$0.82^{+0.09}_{-0.10}$
121209A*	$2.15^{+0.28}_{-0.12}$	$-1.05^{+0.34}_{-0.51}$	$13.78^{+0.03}_{-0.05}$	$0.80^{+0.42}_{-0.13}$
140515A	$3.50^{+0.04}_{-0.04}$	$-1.81^{+0.03}_{-0.04}$	$13.82^{+0.04}_{-0.05}$	$1.85^{+0.77}_{-0.75}$
150911A*	$2.69^{+0.06}_{-0.05}$	$-1.51^{+0.06}_{-0.07}$	$13.80^{+0.01}_{-0.01}$	$8.49^{+4.36}_{-3.91}$
161129A	$3.04^{+0.03}_{-0.04}$	$-1.76^{+0.03}_{-0.03}$	$13.96^{+0.03}_{-0.05}$	$0.90^{+0.06}_{-0.05}$
170202A	$2.74^{+0.05}_{-0.04}$	$-1.20^{+0.06}_{-0.06}$	$13.67^{+0.044}_{-0.03}$	$0.47^{+0.10}_{-0.06}$
170822A*	$3.13^{+0.07}_{-0.05}$	$-1.87^{+0.02}_{-0.02}$	$13.78^{+0.07}_{-0.04}$	$0.98^{+0.27}_{-0.14}$
181110A	$3.08^{+0.11}_{-0.06}$	$-1.55^{+0.03}_{-0.04}$	$13.92^{+0.17}_{-0.04}$	$1.62^{+0.28}_{-0.40}$
190829A	$2.92^{+0.02}_{-0.02}$	$-2.21^{+0.01}_{-0.02}$	$13.86^{+0.02}_{-0.01}$	$9.75^{+0.32}_{-0.44}$
200917A*	$3.02^{+0.09}_{-0.08}$	$-2.09^{+0.08}_{-0.09}$	$13.61^{+0.04}_{-0.04}$	$15.13^{+9.88}_{-8.69}$
201128A*	$2.32^{+0.12}_{-0.11}$	$-1.43^{+0.15}_{-0.19}$	$13.82^{+0.02}_{-0.04}$	$1.20^{+0.15}_{-0.15}$
220117A	$2.74^{+0.07}_{-0.03}$	$-0.92^{+0.05}_{-0.07}$	$13.83^{+0.04}_{-0.03}$	$0.58^{+0.53}_{-0.06}$

Note. [a] No redshift measured of our subsample are mark with [∗], and we adopt $z = 1$ to do the MCMC fits.

of the light cylinder is defined as,

$$R_{\rm L} = \frac{c}{\Omega_{\rm s}}. \tag{11}$$

For simple calculations, one define the fastness parameter as

$$\omega = \frac{\Omega_{\rm s}}{\Omega_{\rm K}(r_{\rm m})} = \left(\frac{r_{\rm m}}{r_{\rm c}}\right)^{3/2}. \tag{12}$$

So that, the net torque exerted on the magnetar by the accretion disc reads as[3]

$$\tau_{\rm acc} = n(\epsilon, \omega)\frac{\mu^2}{r_{\rm m}^3}, \tag{13}$$

where $\epsilon = (r_{\rm m}/R_{\rm L})^{3/2}$, and $n(\epsilon, \omega)$ is the dimensionless torque parameter,

$$n(\epsilon, \omega) = \begin{cases} (2 - 2\epsilon + 6\omega + 3\epsilon^2\omega)/(9\omega), \omega < 1, \\ (2 - 2\epsilon + 6\omega + 3\epsilon^2\omega - 9\omega^2)/(9\omega), \omega \geq 1. \end{cases}$$

The spin evolution is given by the following differential equation,

$$\frac{{\rm d}(I\Omega_{\rm s})}{{\rm d}t} = \tau_{\rm acc} + \tau_{\rm dip}, \tag{14}$$

where $I = 0.35MR_{\rm s}^2$ is the stellar moment of inertia, and $\tau_{\rm dip}$ is the torque due to magnetic dipole radiation and the inclination angle (χ) between the magnetic axis and rotation axis,

$$\tau_{\rm dip} = -\frac{\mu^2\Omega_{\rm s}^3\sin^2\chi}{6c^3} = -\frac{\mu^2\sin^2\chi}{6R_{\rm L}^3}. \tag{15}$$

[3]Here, we do not consider the propellor effects of magnetar, which are suggested by (Piro & Ott 2011), and it is required due to a high-magnetic field of magnetar (e.g. $\sim 5 \times 10^{14}$ G). More details can also refer to (Yu et al. 2024).

By solving above equations, one can get the luminosity of magnetic-dipole-radiation as a function of time (Shapiro & Teukolsky 1983),

$$L_{\rm dip} = \frac{\mu^2\Omega_{\rm s}^4\sin^2\chi}{6c^3} = 9.6 \times 10^{48}\,{\rm erg\,s^{-1}}\sin^2\chi\left(\frac{\mu}{10^{33}\,{\rm G\,cm^3}}\right)^2\left(\frac{P_0}{1\,{\rm ms}}\right)^{-4}. \tag{16}$$

Here, P_0 is the initial period of magnetar.

3.2 Black hole fall-back accretion model

Alternatively, a black hole may be formed as the central engine of long-duration GRBs after the massive star core collapse. The GRB jet can be powered by annihilating between neutrinos and antineutrinos that can carry the accretion energy in the disc or extracting the spin energy of the black hole, which can be tapped by a magnetic field connecting the outer world through the Blandfordd–Znajek (BZ) mechanism (Blandford & Znajek 1977). The fall-back accretion into black hole is also adopted to interpret the late X-ray and optical bumps in the GRB afterglow (Wu et al. 2013; Chen et al. 2017; Lei et al. 2017; Zhao et al. 2021).

The time-scale of fall-back is approximately equal to the free-fall time-scale, $t_{\rm fb} \sim \left(\pi^2 r_{\rm fb}^3/8GM_\bullet\right)^{1/2}$, where $M_\bullet$ is the mass of black hole, $r_{\rm fb}$ is the radius of progenitor. The evolution of the fall-back accretion rate can be described by a broken power-law function of time (Chevalier 1989; MacFadyen et al. 2001),

$$\dot{M} = \dot{M}_{\rm p}\left[\frac{1}{2}\left(\frac{t - t_0}{T_{\rm p} - t_0}\right)^{-s/2} + \frac{1}{2}\left(\frac{t - t_0}{T_{\rm p} - t_0}\right)^{5s/3}\right]^{-\frac{1}{s}}, \tag{17}$$

where t_0 is the beginning time of the fall-back accretion, and s describes the sharpness of the peak. $T_{\rm p}$ and $\dot{M}_{\rm p}$ are the peak time and peak rate of fall-back accretion, respectively.

Based on the results of references (Lee, Wijers & Brown 2000; Li 2000; Wang, Xiao & Lei 2002; McKinney 2005; Lei & Zhang 2011; Chen et al. 2017; Liu, Gu & Zhang 2017), the BZ power from a kerr black hole can be estimated as,

$$\dot{E}_{\rm BZ} = L_{\rm BZ} = 1.7 \times 10^{50} a_\bullet{}^2 M_\bullet{}^2 B_{\bullet,15}{}^2 F(a_\bullet)\,{\rm erg\,s^{-1}}, \quad (18)$$

where $M_\bullet$ is the mass of black hole with unit of $M_\odot$, $B_{\bullet,15} = B_\bullet/10^{15}G$ is the magnetic filed, $a_\bullet = J_\bullet c/(GM_\bullet{}^2)$ and $J_\bullet$ are the spin and angular momentum of black hole, respectively.

$$F(a_\bullet) = [(1+q^2)/q^2][(q+1/q)\arctan q - 1]. \quad (19)$$

Here, $q = a_\bullet/(1+\sqrt{1-a_\bullet^2})$. The range of spin parameter is $0 \le a_\bullet \le 1$, so that, one has $2/3 \le F(a_\bullet) \le \pi - 2$. By assuming that the magnetic field pressure of the BH and the ram pressure ($P_{\rm ram}$) of the innermost parts of an accretion flow are in balance, one has Moderski, Sikora & Lasota (1997)

$$\frac{B_\bullet^2}{8\pi} = P_{\rm ram} \sim pc^2 \sim \frac{\dot{M}c}{4\pi r_\bullet^2}, \quad (20)$$

where $r_\bullet = (1+\sqrt{1-a_\bullet^2})r_{\rm g}$ is the radius of the BH horizon and $r_{\rm g} = GM_\bullet/c^2$. Combining with equations (17), (18), and (19), $B_\bullet$ and $L_{\rm BZ}$ can be rewritten as

$$B_\bullet \approx 7.4 \times 10^{16} \dot{M}^{1/2} M_\bullet^{-1} \left(1+\sqrt{1-a_\bullet^2}\right)^{-1} G. \quad (21)$$

$$L_{\rm BZ} = 9.3 \times 10^{53} a_\bullet^2 \dot{M} X(a_\bullet)\,{\rm erg\,s^{-1}}, \quad (22)$$

where

$$X(a_\bullet) = F(a_\bullet)/\left(1+\sqrt{1-a_\bullet^2}\right)^2. \quad (23)$$

Within the scenario of the energy conservation and angular momentum conservation, there are two teams of the evolution equation of BH in the BZ model, i.e., spin-up by accretion and spin-down by the BZ mechanism (Wang et al. 2002),

$$\frac{{\rm d}M_\bullet c^2}{{\rm d}t} = \dot{M}c^2 E_{\rm ms} - L_{\rm BZ} \quad (24)$$

$$\frac{{\rm d}J_\bullet}{{\rm d}t} = \dot{M}L_{\rm ms} - T_{\rm BZ} \quad (25)$$

$$\frac{{\rm d}a_\bullet}{{\rm d}t} = (\dot{M}L_{\rm ms} - T_{\rm BZ})c/(GM_\bullet{}^2) - 2a_\bullet(\dot{M}c^2E_{\rm ms} - L_{\rm BZ})/(M_\bullet c^2), \quad (26)$$

where $T_{\rm BZ}$ is the total magnetic torque that applied to BH (Li 2000; Lei & Zhang 2011; Lei et al. 2017),

$$T_{\rm BZ} = \frac{4GM_\bullet L_{\rm BZ}\left(1+\sqrt{1-a_\bullet^2}\right)}{a_\bullet c^3}. \quad (27)$$

In equations (23) and (24), $E_{\rm ms}$ and $L_{\rm ms}$ are the specific energy and angular momentum, which are corresponding to the innermost radius ($r_{\rm ms}$) of the disc, and defined as following,

$$E_{\rm ms} = \frac{4\sqrt{R_{\rm ms}} - 3a_\bullet}{\sqrt{3}R_{\rm ms}} \quad (28)$$

$$L_{\rm ms} = \frac{GM_\bullet}{c}\frac{(6\sqrt{R_{\rm ms}} - 4a_\bullet)}{\sqrt{3R_{\rm ms}}} \quad (29)$$

and $R_{\rm ms}$ can be referenced from Bardeen, Press & Teukolsky (1972),

$$R_{\rm ms} = \frac{r_{\rm ms}}{r_{\rm g}} = 3 + Z_2 - [(3-Z_1)(3+Z_1+2Z_2)]^{1/2}. \quad (30)$$

Here, $Z_1 \equiv 1 + (1-a_\bullet^2)^{1/3}[(1+a_\bullet)^{1/3} + (1-a_\bullet)^{1/3}]$ and $Z_2 \equiv \left(3a_\bullet^2 + Z_1^2\right)^{1/2}$ $(0 \le a_\bullet \le 1)$.

4 THE FITTING RESULTS OF MODELS APPLICATION TO OUR SELECTED SAMPLE

In this section, we assume that the early and late bumps of X-ray afterglow are related to the fall-back accretion of magnetar and black hole, respectively. Then, we adopt the fall-back accretion of magnetar and black hole to fit the early and late bumps of X-ray afterglow with Monte Carlo Markov Chain (MCMC) method, respectively. Due to no redshift measurement of some GRBs in our sample, we adopt $z = 1$ to do the calculations instead of no redshift-measured GRBs.[4]

4.1 Fall-back accretion of magnetar to early bumps

Based on the criteria of sample selected and the distribution of peak time for both early and late X-ray bumps, there are 19 long-duration GRBs, which are identified as the 'early bump' category, and 12 of which have redshift measurements. So that, we attempt the fall-back accretion of magnetar model to fit the those GRBs with early bumps. Considering the poorly understanding the equation of state of magnetar, we adopt the typical values of mass and radius of magnetar as $1.4\,M_\odot$ and 10 km to do the fits, respectively. Moreover, we also fix $\sin\chi = 0.5$ in our calculations due to unknown inclination angle of the magnetic axis to the rotation axis (Dai & Liu 2012).

If this is the case, there are four free parameters of fall-back accretion of magnetar, e.g. t_1, $\eta_{\rm mag}$, B_0, and P_0. Moreover, by considering the contributions from the initial steep decay segment (tail emission of prompt emission) and afterglow with power-law decay component (e.g. external shock) to the fits, we also simultaneously fit the light curves with all three components above (e.g. steep decay, afterglow, and fall-back accretion). Then, we adopt the MCMC method with PYTHON code to fit the data. In our fitting, we use a PYTHON module EMCEE to get best-fit values and uncertainties of free parameters (Foreman-Mackey et al. 2013). The allowed range of the four free parameters are set as $\log(t_1)\epsilon[2.15, 3.36]$ s, $\log(\eta_{\rm mag})\epsilon[-2.16, -1.05]$, $\log(B_0)\epsilon[13.58, 13.96]$; and $P_0\epsilon[0.8, 8.5]$ ms. Fig. 2 shows two examples of best fitted light curves and the corner plots of free parameters posterior probability distribution for the fall-back accretion model.[5] The results of fits for all 21 early bumps are listed in Table 2.

It is worth testing that what are the distributions of the values for t_1, B_0, and P_0. Fig. 3 shows the distributions of those fitting values. It is found that those values are obeyed the normal (P_0) or lognormal (t_1 and B_0) distributions with $\log(t_1) = (3.01 \pm 0.12)$ s, $\log(B_0) = (13.77 \pm 0.03)$ G, and $P_0 = (1.04 \pm 0.05)$ ms, respectively. Moreover, the distribution of $\eta_{\rm mag}$ is range of [0.6, 17 per cent]. In any case, based on the MCMC fitting results, one can see that the early bumps of our sample are well fitted by fall-back accretion of magnetar model, and all free parameters can be constrained very well. The values of those parameters also fall into a reasonable range.

4.2 Fall-back accretion of black hole to late bumps

Based on the bimodal distribution of peak time of bumps in our sample, there are 9 GRBs that are identified as 'late bump' category, and 5 of which have redshift measurements. So that, we apply the fall-back accretion of black hole model and the afterglow component to fit

[4]Jakobsson et al. (2006) found that the mean redshift is $z \sim 2.8$ for a small GRB samples. The different pseudo-redshift that we adopt is indeed making a huge difference of inferred energetics, and it can affect the inferred parameters of fall-back accretion in both magnetar and black hole.

[5]https://astro.gxu.edu.cn/info/1062/2244.htm

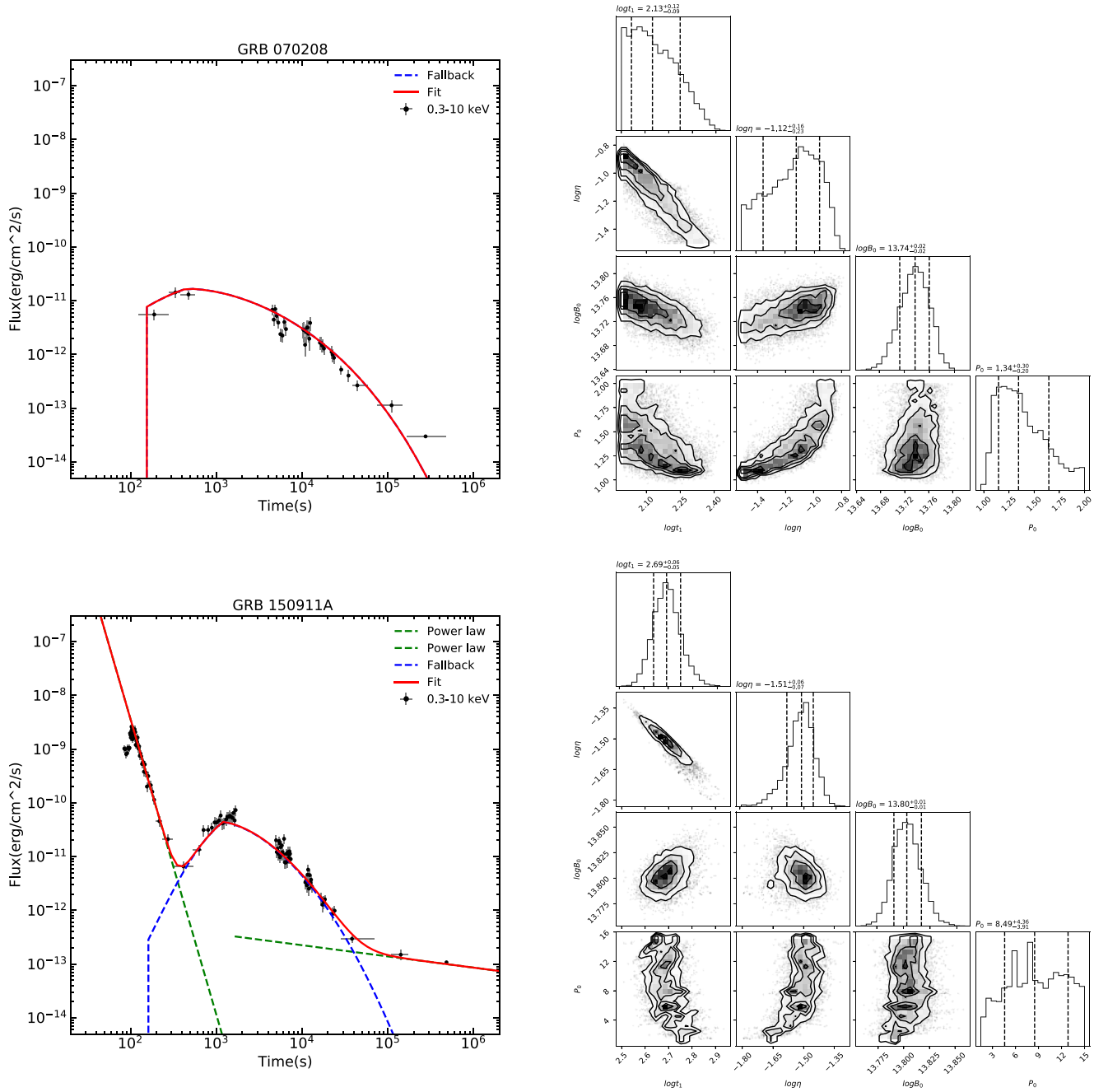

Figure 2. Fall-back accretion of magnetar modelling results of two examples for the early bumps of X-ray afterglow (left) and the corner plots of the free parameters posterior probability distribution.

those GRBs with late bumps. Here, we adopt the beginning time (t_s) and ending time of the bumps (t_e) as the beginning time and ending time of the fall-back accretion (Zhao et al. 2021). The initial mass and spin of black hole are fixed as $M_0 = 3M_\odot$ and $a_0 = 0.9$, respectively (Lei et al. 2017). Meanwhile, due to uncertainty efficiency and jet opening angle of GRBs, we take $\eta_{BH} = 0.01$ and $f_b = 0.01$ during the calculations. We define a dimensionless parameter as peak of fall-back accretion rate $\dot{m}_p$ ($\dot{m}_p = \dot{M}_p/M_\odot\,s^{-1}$), and T_p is the peak time when the fall-back accretion rate $\dot{m}_p$ reaches at the peak. Here, we only focus on free parameters of fall-back accretion of black hole, e.g. $\dot{m}_p$, T_p, and s.

We then adopt the MCMC method with PYTHON code to fit the data of those 9 GRBs with late bumps. The ranges of the free parameters are set as follows: $\log(\dot{m}_p)\epsilon[-10, 0]$, $s\epsilon[0, 5]$ and $T_p\epsilon[t_s, t_e]$. Two examples of best-fitted light curves for the late-bumps and the the corner plots of free parameters posterior probability distribution are shown in Fig. 4, and the full fitting results can be found in footnote 5. The results of fits for all 9 late bumps are listed in Table 3. It is found that the the distributions of $\log T_p$, s, and $\log \dot{m}_p$ are range of [4.26, 4.88], [0.33, 1.53], and [−7.77, −5.73], respectively (see Fig. 5).

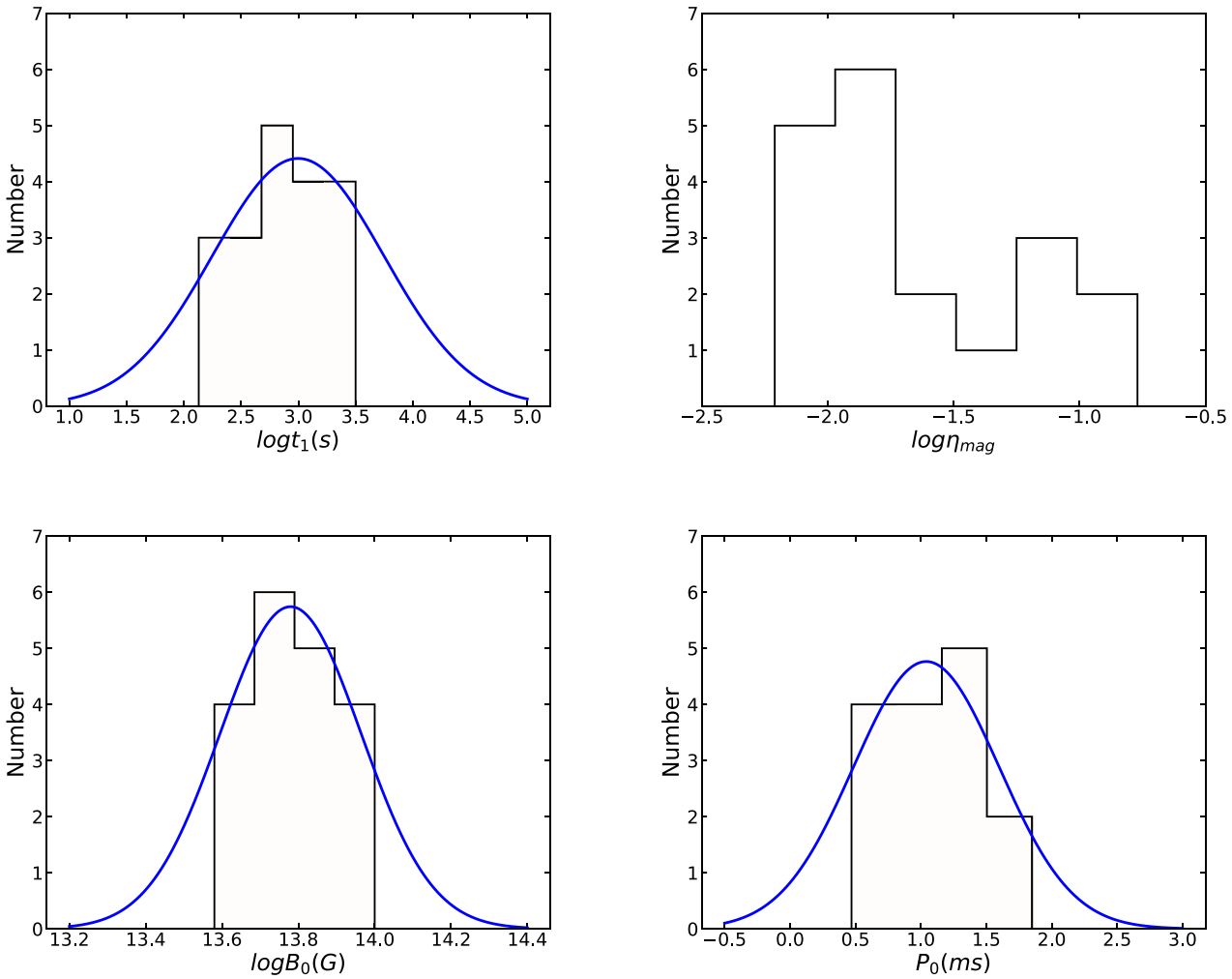

Figure 3. Distributions of free parameters for early bumps with fall-back accretion of magnetar model. The solid bule lines are the Gaussian fits.

Furthermore, we also calculate the total mass of the accretion ($M_{\rm acc}$) in the fall-back process when we do the integral of time for equation (15), and the fall-back radius can also be estimated as,

$$R_{\rm fb} \approx 3.5 \times 10^{10} (M_\bullet/3\,{\rm M}_\odot)^{1/3} (t_{\rm fb}/360\,{\rm s})^{2/3} {\rm cm}. \quad (31)$$

The derived physical parameters of $M_{\rm acc}$ and $R_{\rm fb}$ are also listed in Table 3. We also do the distributions of the derived physical parameters, and it is found that the distribution of $M_{\rm acc}$ is range of $[4 \times 10^{-4}, 1.8 \times 10^{-2}]\,{\rm M}_\odot$. The fall-back radius is range of $[1.04, 4.23] \times 10^{11}$ cm, which is consistent with the typical radius of a Wolf–Rayet star. In any case, the late bumps of our sample can be well fitted by fall-back accretion of black hole model, and the values of those parameters fall into a reasonable range.

Moreover, it is notice that both accretion rate and accretion mass in this work are much lower than that of in supernova explosion at the same time (Moriya et al. 2019). That is because the adopted mass of progenitor star and black hole in Moriya et al. (2019) are much larger than that of what we adopt.

5 CONCLUSION AND DISCUSSION

The central engine of long-duration GRBs remain an open question (Zhang 2011), and some characteristic of afterglow emission (i.e. X-ray re-brightening) may take a clue to understand the naturally central engine and progenitor of GRBs. In this paper, we systemically search for long-duration GRBs that consist of bumps in X-ray afterglow detected by *Swift*/XRT between 2005 January and 2023 July, and found that 28 candidate GRBs showing X-ray bumps in their afterglow.

More interestingly, we find that the peak time of the X-ray bumps in our sample exhibits bimodal distribution, and defined as 'early' and 'late' bumps with division line at $t = 7190$ s, e.g. early bumps with $t_{\rm p} < 7190$ s, and late bumps with $t_{\rm p} > 7190$ s, respectively. We proposed that the long-duration GRBs with an early (or late) bumps may be originated from the fall-back accretion onto a new-born magnetar (or black hole). By adopting MCMC method to fit the early (or late) bumps of X-ray afterglow with the fall-back accretion of magnetar (or black hole), we are able to reach several interesting results.

(i) Both early and late bumps of X-ray afterglow in our sample can be well fitted by the fall-back accretion of magnetar and black hole, respectively. The values of parameters for those two models also fall into a reasonable range.

(ii) The initial surface magnetic filed and period of magnetars for most early bumps are clustered around 5.88×10^{13} G and 1.04 ms, respectively.

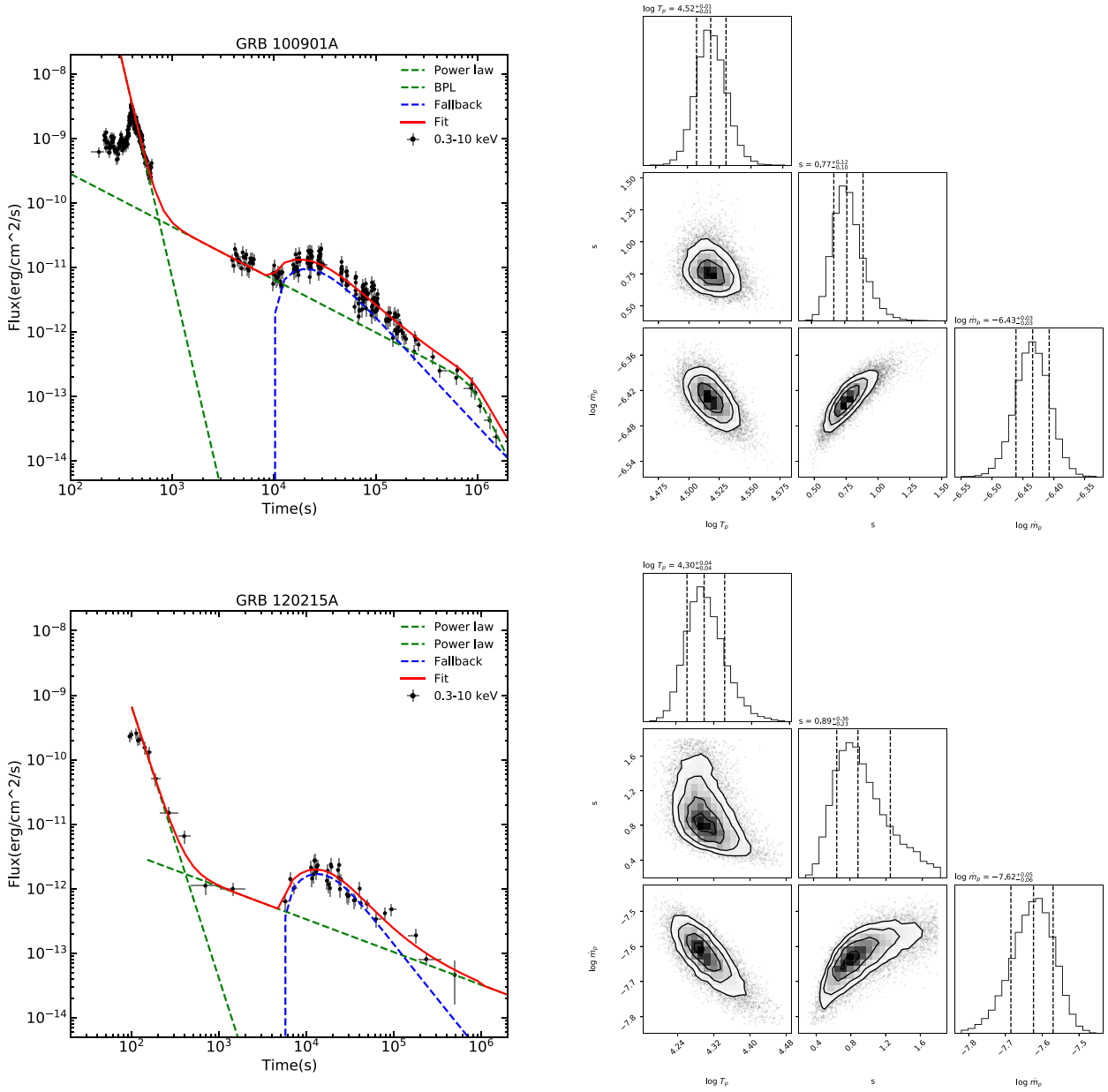

Figure 4. Fall-back accretion of black hole modelling results of two examples for the late bumps of X-ray afterglow (left) and the corner plots of the free parameters posterior probability distribution.

(iii) The fall-back accretion rate reaches its peak value (1.7×10^{-8}–1.9×10^{-6}) $M_\odot\ s^{-1}$, and the derived accretion mass of black hole for late bumps is range of $[4 \times 10^{-4}, 1.8 \times 10^{-2}]\ M_\odot$. The typical fall-back radius is distributed range of $[1.04, 4.23] \times 10^{11}$ cm, which is consistent with the typical radius of a Wolf–Rayet star.

A very interesting question is whether the early bumps can also be interpreted by fall-back accretion of black hole. In order to test this possibility, we invoke the same MCMC method to fit the early bumps of X-ray afterglow in our sample by using the fall-back of black hole central engine model. We find that most early bumps (15 out of 19) can be fitted by the fall-back accretion of black hole model, but require a larger accretion rate. It means that the fall-back accretion of black hole model cannot be ruled out to interpret the early bumps. On the contrary, we also invoke the fall-back accretion magnetar model to fit the late bumps of X-ray afterglow in our sample. We find that the fall-back accretion magnetar model is very difficult to fit the late bumps, such as the parameters of model are not convergent, or unreasonable distribution of model parameters. It suggest that the fall-back accretion magnetar model is disfavoured by the late bumps of X-ray afterglow in our sample.

In addition, several proposed models are also invoke to interpret the re-brightening feature in afterglow of GRBs, e.g. the fireball decelerated by the ambient medium (Sari & Piran 1999; Kobayashi & Zhang 2007), the density bumps or voids in the circumburst medium (Dai & Lu 2002; Lazzati et al. 2002), a refreshed shock (Zhang & Mészáros 2002; Björnsson, Gudmundsson & Jóhannesson 2004), a structured jet with off-axis (Berger et al. 2003; Nakar, Piran & Waxman 2003; Huang et al. 2004; Panaitescu & Vestrand 2008; Guidorzi et al. 2009; Margutti et al. 2010), a long-lasting reverse

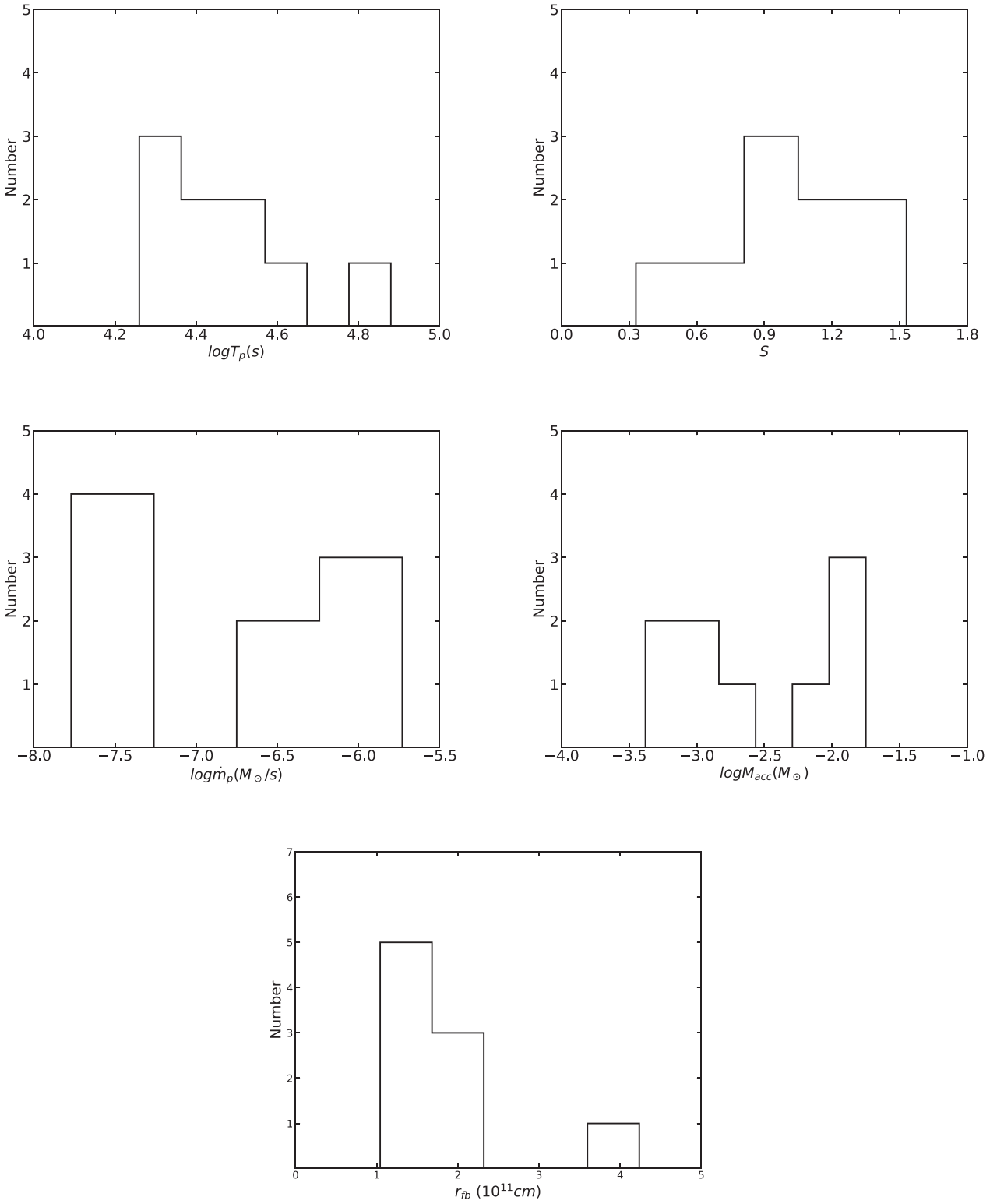

Figure 5. Distributions of free parameters for late bumps with fall-back accretion of black hole model.

shock model (Uhm et al. 2012), the existence two component jets (Huang et al. 2004; Wu et al. 2005; Racusin et al. 2008).

Moreover, one needs to clarify that the bimodal distribution of peak times for our sample can be affected by the selection effect. It is possible that the number of what we selected sample is a sub-class of total GRBs observed by *Swift*/XRT. On the other hand, the bimodal distribution of peak times is also possible affected by the sheltering from Earth, namely, the dip of distribution is possible caused by the selection effect due to sheltered time from Earth. Also, the derived parameters of early bumps (or late bumps) with magnetar

Table 3. The MCMC fitting and calculated results of late bump subsample with fall-back accretion of black hole.

GRB Name	$\log(T_{\rm p})$ (s)	s	$\log(\dot{m}_{\rm p})$ ($M_\odot$ s^{-1})	$\log(M_{\rm acc})$ ($M_\odot$)	$R_{\rm fb}$ (10^{11} cm)
071010A	$4.88^{+0.03}_{-0.02}$	$1.48^{+0.65}_{-0.57}$	$-7.77^{+0.06}_{-0.08}$	-2.99	4.23
081028	$4.44^{+0.01}_{-0.01}$	$1.22^{+0.25}_{-0.19}$	$-5.79^{+0.03}_{-0.03}$	-1.75	1.21
100901A	$4.52^{+0.01}_{-0.01}$	$0.77^{+0.12}_{-0.10}$	$-6.51^{+0.03}_{-0.03}$	-2.05	1.74
120215A*	$4.30^{+0.04}_{-0.04}$	$0.87^{+0.36}_{-0.23}$	$-7.69^{+0.05}_{-0.06}$	-3.38	1.26
120326A	$4.67^{+0.03}_{-0.02}$	$0.84^{+0.21}_{-0.16}$	$-6.24^{+0.03}_{-0.03}$	-1.85	1.93
130807A*	$4.26^{+0.06}_{-0.05}$	$1.12^{+0.67}_{-0.38}$	$-7.42^{+0.08}_{-0.08}$	-3.14	1.04
131018A*	$4.47^{+0.08}_{-0.07}$	$0.33^{+0.10}_{-0.07}$	$-7.48^{+0.05}_{-0.06}$	-2.86	1.19
150626B*	$4.35^{+0.02}_{-0.02}$	$1.53^{+0.52}_{-0.36}$	$-6.74^{+0.03}_{-0.03}$	-2.62	2.02
230414B	$4.49^{+0.06}_{-0.04}$	$0.64^{+0.30}_{-0.22}$	$-7.38^{+0.09}_{-0.11}$	-3.38	1.09

Note.[a] No redshift measured of our subsample are mark with [∗], and we adopt $z = 1$ to do the MCMC fits and calculations.

(or black hole) fall-back model are dependent on the equation of state of neutron star (or initial mass of black hole) We hope that more observational data in X-ray band (i.e. Einstein probe) can be obtained in the future to identify the signature of central engine of GRBs.

ACKNOWLEDGEMENTS

We acknowledge the use of the public data from the UK Swift Science Data Center. This work is supported by the Guangxi Science Foundation (grant No. 2023GXNSFDA026007), the Natural Science Foundation of China (grant Nos. 11922301 and 12133003), the Program of Bagui Scholars Program (LHJ), and the Guangxi Talent Program ('Highland of Innovation Talents').

DATA AVAILABILITY

This is the theoretical work, and there are no new data associated with this article. If one needs to adopt the data in this article, it should be cited this reference paper.

REFERENCES

Agui Fernandez J. F., Thoene C. C., de Ugarte Postigo A., Scarpa R., Marante A., Cabrera Lavers A. L., 2023, GRB Coordinates Network, 33629, 1
Bardeen J. M., Press W. H., Teukolsky S. A., 1972, ApJ, 178, 347
Berger E. et al., 2003, Nature, 426, 154
Berger E., Foley R., Simcoe R., Irwin J., 2008, GRB Coordinates Network, 8434, 1
Björnsson G., Gudmundsson E. H., Jóhannesson G., 2004, ApJ, 615, L77
Blandford R. D., Znajek R. L., 1977, MNRAS, 179, 433
Burrows D. N. et al., 2005, Space Sci. Rev., 120, 165
Cano Z., Malesani D., de Ugarte Postigo A., Izzo L., Thoene C. C., Castro-Rodriguez N., 2016, GRB Coordinates Network, 20245, 1
Chen W.-X., Beloborodov A. M., 2007, ApJ, 657, 383
Chen W., Xie W., Lei W.-H., Zou Y.-C., Lü H.-J., Liang E.-W., Gao H., Wang D.-X., 2017, ApJ, 849, 119
Chevalier R. A., 1989, ApJ, 346, 847
Chincarini G. et al., 2007, ApJ, 671, 1903
Chornock R., Perley D. A., Cobb B. E., 2009, GRB Coordinates Network, 10100, 1
Chornock R., Berger E., Fox D., Levan A. J., Tanvir N. R., Wiersema K., 2010, GRB Coordinates Network, 11164, 1
Chornock R., Fox D. B., Berger E., 2014, GRB Coordinates Network, 16269, 1
Cucchiara A., Fox D. B., Cenko S. B., Price P. A., 2007, GRB Coordinates Network, 6083, 1
Cucchiara A. et al., 2011, ApJ, 736, 7
Dai Z. G., Liu R.-Y., 2012, ApJ, 759, 58
Dai Z. G., Lu T., 1998a, Phys. Rev. Lett., 81, 4301
Dai Z. G., Lu T., 1998b, A&A, 333, L87
Dai Z. G., Lu T., 2002, ApJ, 565, L87
Eichler D., Livio M., Piran T., Schramm D. N., 1989, Nature, 340, 126
Evans P. A. et al., 2007, A&A, 469, 379
Fan Y.-Z., Xu D., 2006, MNRAS, 372, L19
Foreman-Mackey D., Hogg D. W., Lang D., Goodman J., 2013, PASP, 125, 306
Fynbo J. P. U. et al., 2006, A&A, 451, L47
Guidorzi C. et al., 2009, A&A, 499, 439
Huang Y. F., Wu X. F., Dai Z. G., Ma H. T., Lu T., 2004, ApJ, 605, 300
Jakobsson P. et al., 2006, A&A, 447, 897
Kobayashi S., 2000, ApJ, 545, 807
Kobayashi S., Zhang B., 2007, ApJ, 655, 973
Kumar P., Narayan R., Johnson J. L., 2008, Science, 321, 376
Lazzati D., Rossi E., Covino S., Ghisellini G., Malesani D., 2002, A&A, 396, L5
Lee H. K., Wijers R. A. M. J., Brown G. E., 2000, Phys. Rep., 325, 83
Lei W.-H., Zhang B., 2011, ApJ, 740, L27
Lei W.-H., Zhang B., Liang E.-W., 2013, ApJ, 765, 125
Lei W.-H., Zhang B., Wu X.-F., Liang E.-W., 2017, ApJ, 849, 47
Li L.-X., 2000, Phys. Rev. D, 61, 084016
Liang E. W. et al., 2006, ApJ, 646, 351
Liang E.-W., Zhang B.-B., Zhang B., 2007, ApJ, 670, 565
Lipunov V. et al., 2019, GRB Coordinates Network, 25573, 1
Liu T., Gu W.-M., Zhang B., 2017, New A Rev., 79, 1
Lü H.-J., Zhang B., 2014, ApJ, 785, 74
Lü H.-J., Zhang B., Lei W.-H., Li Y., Lasky P. D., 2015, ApJ, 805, 89
Lü H.-J., Zou L., Lan L., Liang E.-W., 2018, MNRAS, 480, 4402
Lü H.-J. et al., 2022, ApJ, 931, L23
Lyons N., O'Brien P. T., Zhang B., Willingale R., Troja E., Starling R. L. C., 2010, MNRAS, 402, 705
MacFadyen A. I., Woosley S. E., 1999, ApJ, 524, 262
MacFadyen A. I., Woosley S. E., Heger A., 2001, ApJ, 550, 410
Malesani D., Kruehler T., Perley D., Fynbo J. P. U., Xu D., Milvang-Jensen B., Goldoni P., Schulze S., 2013, GRB Coordinates Network, 14225, 1
Margutti R., Guidorzi C., Chincarini G., Bernardini M. G., Genet F., Mao J., Pasotti F., 2010, MNRAS, 406, 2149
McKinney J. C., 2005, ApJ, 630, L5
Mészáros P., 2002, ARA&A, 40, 137
Mészáros P., Rees M. J., 1997, ApJ, 476, 232
Metzger B. D. et al., 2010, MNRAS, 406, 2650
Moderski R., Sikora M., Lasota J. P., 1997, in Ostrowski M., Sikora M., Madejski G., Begelman M., eds, Relativistic Jets in AGNs. p. 110, preprint (arXiv:astro-ph/9706263)
Moriya T. J., Müller B., Chan C., Heger A., Blinnikov S. I., 2019, ApJ, 880, 21

Nakar E., Piran T., Waxman E., 2003, J. Cosmol. Astropart. Phys., 2003, 005
Narayan R., Piran T., Kumar P., 2001, ApJ, 557, 949
Nousek J. A. et al., 2006, ApJ, 642, 389
O'Brien P. T. et al., 2006, ApJ, 647, 1213
Palmerio J., Kruehler T., Malesani D., Fynbo J. P. U., 2017, GRB Coordinates Network, 20589, 1
Palmerio J. et al., 2022, GRB Coordinates Network, 31480, 1
Panaitescu A., Vestrand W. T., 2008, MNRAS, 387, 497
Pe'er A., Mészáros P., Rees M. J., 2006, ApJ, 642, 995
Perley D. A., Malesani D. B., Fynbo J. P. U., Heintz K. E., Kann D. A., D'Elia V., Izzo L., Tanvir N. R., 2018, GRB Coordinates Network, 23421, 1
Piro A. L., Ott C. D., 2011, ApJ, 736, 108
Popham R., Woosley S. E., Fryer C., 1999, ApJ, 518, 356
Prochaska J. X., Perley D. A., Modjaz M., Bloom J. S., Poznanski D., Chen H. W., 2007, GRB Coordinates Network, 6864, 1
Racusin J. L. et al., 2008, Nature, 455, 183
Rees M. J., Meszaros P., 1994, ApJ, 430, L93
Rees M. J., Mészáros P., 2005, ApJ, 628, 847
Rowlinson A. et al., 2010, MNRAS, 409, 531
Rowlinson A., O'Brien P. T., Metzger B. D., Tanvir N. R., Levan A. J., 2013, MNRAS, 430, 1061
Sari R., Piran T., 1999, ApJ, 517, L109
Sari R., Piran T., Narayan R., 1998, ApJ, 497, L17
Shapiro S. L., Teukolsky S. A., 1983, Black holes, white dwarfs and neutron stars. The physics of compact objects.Wiley-Interscience Publication, New York
Soderberg A. M., Berger E., Ofek E., 2005, GRB Coordinates Network, 4186, 1
Tello J. C., Sanchez-Ramirez R., Gorosabel J., Castro-Tirado A. J., Rivero M. A., Gomez-Velarde G., Klotz A., 2012, GRB Coordinates Network, 13118, 1
Thompson C., 1994, MNRAS, 270, 480
Troja E. et al., 2007, ApJ, 665, 599
Troja E., Piro L., Vasileiou V., Omodei N., Burgess J. M., Cutini S., Connaughton V., McEnery J. E., 2015, ApJ, 803, 10
Uhm Z. L., Zhang B., Hascoët R., Daigne F., Mochkovitch R., Park I. H., 2012, ApJ, 761, 147
Usov V. V., 1992, Nature, 357, 472
Wang D. X., Xiao K., Lei W. H., 2002, MNRAS, 335, 655
Woosley S. E., 1993, ApJ, 405, 273
Wu X. F., Dai Z. G., Huang Y. F., Lu T., 2005, MNRAS, 357, 1197
Wu X.-F., Hou S.-J., Lei W.-H., 2013, ApJ, 767, L36
Yi S.-X., Xi S.-Q., Yu H., Wang F. Y., Mu H.-J., Lü L.-Z., Liang E.-W., 2016, ApJS, 224, 20
Yu Y. B., Huang Y. F., Wu X. F., Xu M., Geng J. J., 2015, ApJ, 805, 88
Yu W.-Y., Lü H.-J., Yang X., Lan L., Yang Z., 2024, ApJ, 962, 6
Zhang B., 2011, Comptes Rendus Physique, 12, 206
Zhang B., 2018, The Physics of Gamma-Ray Bursts
Zhang D., Dai Z. G., 2008, ApJ, 683, 329
Zhang D., Dai Z. G., 2009, ApJ, 703, 461
Zhang B., Mészáros P., 2001, ApJ, 552, L35
Zhang B., Mészáros P., 2002, ApJ, 566, 712
Zhang B., Mészáros P., 2004, Int. J. Mod. Phys. A, 19, 2385
Zhang B., Yan H., 2011, ApJ, 726, 90
Zhang B., Fan Y. Z., Dyks J., Kobayashi S., Mészáros P., Burrows D. N., Nousek J. A., Gehrels N., 2006, ApJ, 642, 354
Zhang B., Lü H.-J., Liang E.-W., 2016, Space Sci. Rev., 202, 3
Zhao L., Gao H., Lei W., Lan L., Liu L., 2021, ApJ, 906, 60
Zhong S.-Q. et al., 2016, ApJ, 831, 5

This paper has been typeset from a TEX/LATEX file prepared by the author.